ELSEVIER

Thermochimica Acta 304/305 (1997) 125–136

thermochimica acta

Heat-capacity determination by temperature-modulated DSC and its separation from transition effects[1,2]

B. Wunderlich[3,*], A. Boller, I. Okazaki[4], K. Ishikiriyama[5]

Department of Chemistry, The University of Tennessee, Knoxville, TN, 37996-1600, USA

Received 21 July 1996; accepted 14 March 1997

Abstract

Temperature-modulated calorimetry offers three methods of establishing heat capacity: (1) the traditional method of scanning thermal analysis by finding the heat flow into the sample during a measured temperature increase: (2) the quasi-isothermal method by finding the maximum amplitude of the periodic heat flow in response to a temperature modulation at a constant base temperature; and (3) the pseudo-isothermal analysis of a temperature-modulated scanning experiment by subtracting the effect due to the underlying (usually constant) heating rate and evaluating the effect due to the modulation as in a quasi-isothermal experiment. The background, advantages, and limitations of the three methods are discussed along with the possibility of establishing apparent heat capacities in dynamic systems, and the separation of heat capacities from phase transitions. © 1997 Elsevier Science B.V.

Keywords: Differential scanning calorimetry (DSC); Glass transition; Heat capacity; Melting transition; Temperature-modulated calorimetry (TMC)

1. Introduction

Heat capacity and transition enthalpies (latent heats) are the basic thermodynamic quantities available through calorimetry. Precision calorimetry started at the turn of the century with adiabatic calorimetry [1]. This was followed in the middle of the century by differential scanning calorimetry (DSC), a much faster working method with much smaller samples [2]. Although another method, alternating current calorimetry (AC calorimetry), was developed some time ago [3], its application was limited. Presently, the method of temperature-modulated calorimetry (TMC), is flourishing because of its application to DSC. It broadens the experimental approaches to the measurement of heat capacity. In this paper, measurement of heat capacity will be discussed, and the relation to effects seen during transitions analyzed. Reference is made to the temperature-modulated differential scanning calorimetry (TMDSC), based on

*Corresponding author.

[1]Presented at the Fourth Lähnwitz Seminar 6/96.

[2]The submitted manuscript has been authored by a contractor of the U.S. Government under the contract No. DE-AC05-96OR22464. Accordingly, the U.S. Government retains a non-exclusive, royalty-free license to publish, or reproduce the published form of this contribution, or allow others to do so, for U.S. Government purposes.

[3]Chemical and Analytical Sciences Division, Oak Ridge National Laboratory, Oak Ridge, TN 37831-6197, USA.

[4]On leave from Toray Industries, Inc, Otsu, Shiga 520, Japan.

[5]On leave from Toray Research Center, Inc., Otsu, Shiga 520, Japan.

PII S0040-6031(97)00184-6

heat flux, as it is available through TA Instrument (modulated differential scanning calorimeter, MDSC™) [4]. In this MDSC, the modulation is controlled at the sample thermocouple. Differences are expected on modulation at the reference or furnace thermocouples, as well as on modulating power-compensation calorimeters.

2. Methods of heat capacity measurements

The definition of heat capacity at constant pressure, C_p, is given by:

$$C_p \equiv \frac{dQ}{dT} = \left(\frac{\partial H}{\partial T}\right)_{p,n} \tag{1}$$

with Q representing the heat exchanged, H the enthalpy, and the subscripts 'p' and 'n' signify the conditions of constant pressure and composition. The dimension of C_p is $J\,K^{-1}\,mol^{-1}$, or, for the specific heat capacity $J\,K^{-1}\,g^{-1}$. The basic measurement involves, thus, the determination of the amount of heat needed to raise the temperature by a given amount $(\Delta Q/\Delta T)$.

Classically, the measurement of heat capacity is done with an adiabatic calorimeter [1]. Even today, adiabatic calorimetry is the most precise method of measurement in the (10–300) K temperature range (possible precision ±0.1%), and practically the only method used in the (10–150) K range [5]. In an adiabatic calorimeter, an attempt is made to follow the stepwise temperature changes, ΔT, of an internally heated calorimeter in well-controlled, adiabatic surroundings. Corrections must be made for ΔQ due to the positive or negative heat flux caused by deviations from the adiabatic condition, and for ΔT due to temperature drifts of the calorimeter. The specific heat capacity c_p thus becomes:

$$c_{p(sample)} = \frac{\Delta Q_{corrected} - C'\Delta T_{corrected}}{\Delta T_{corrected} \times m_{sample}} \tag{2}$$

where C' is the heat capacity of the empty calorimeter, its 'water value,' and m, the mass of the sample [5]. Evaluation of the corrections is the most time-consuming part of the measurement and at the heart of good calorimetry (i.e. for measurements with better than ±1% precision). It involves calibration of temperature and heat flow of the calorimeter outside of the heating cycle.

Modern control and measurement technology permitted, some 30 years ago, to miniaturize the calorimeter to measure milligram quantities in a continuous scanning mode, and to change from an adiabatic to an isoperibol environment [2]. Twin calorimetry was needed to simplify the heat flux correction by measuring in a differential mode between a sample and a reference calorimeter. In a symmetric setup, the extraneous heat-flux difference could be minimized and the remaining, small imbalance corrected for. This type of instrument is the well-known differential scanning calorimeter, DSC. Under the usual condition where sample and reference calorimeters (often aluminum pans) are identical, and the reference pan is empty, one finds the heat capacity as:

$$mc_p \approx \frac{K\langle\Delta T\rangle}{\langle q\rangle} \tag{3}$$

where K is the Newton's law constant, $\langle\Delta T\rangle$ the temperature difference between reference and sample $(T_r - T_s)$, and $\langle q\rangle$ the constant heating rate. Both quantities are enclosed in angular brackets, $\langle\ \rangle$, to indicate that in the case of TMC (see below) these quantities the sliding averages over a $\pm 1/2$ modulation cycle. Eq. (3) is exact if the sample and reference calorimeters are heated at the same rate (steady state and constant c_p, resulting in a horizontal DSC-curve). For the case of changing heating rate of the sample due to a slowly changing heat capacity, easy corrections are available [5], but often neglected for measurements with precisions in the range of ±3%.

In TMDSC, one uses a sinusoidal or other periodic temperature modulation that is superimposed on the underlying heating rate $\langle q\rangle$ [4]. The sample temperature is, under these conditions, changing as given by:

$$T_s(t) = T_0 + \langle q\rangle t - \langle q\rangle \frac{C_s}{K} + A\sin(\omega t - \varepsilon) \tag{4}$$

where T_0 is the temperature at the start of the experiment, C_s the heat capacity of the sample calorimeter (sample + pan), A the maximum amplitude of the sample-temperature modulation, and ω the modulation frequency $2\pi/p$ (p = modulation period in seconds). Analogous equations hold for the reference

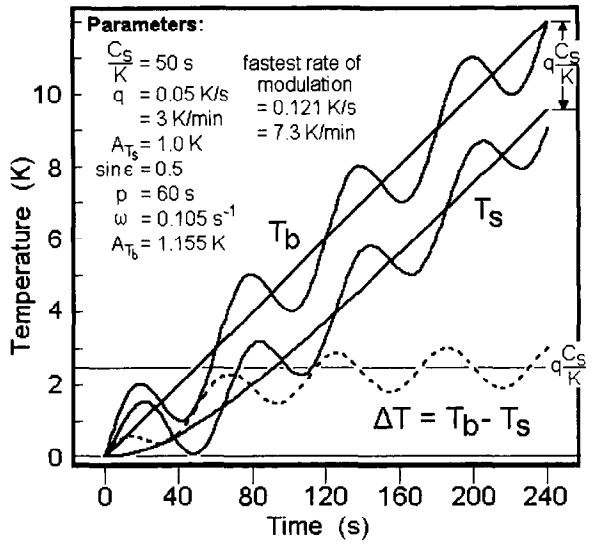

Fig. 1. Change of block and sample temperatures at the beginning of a TMDSC experiment. The averages apply to standard DSC.

temperature, T_r (maximum amplitude A_t and phase shift ϕ) and the temperature difference, $\Delta T = T_r - T_s$ (maximum amplitude A_Δ and phase shift δ) [6]. The standard DSC can be thought of as TMDSC without modulation ($A = 0$).

The conditions for the calorimeter to approach a steady state have been explored [7]. A typical approach to steady state of the sample temperature T_s at the beginning of a run is illustrated in Fig. 1. The standard DSC case is given by the heavy lines without modulation and TMDSC is given by the modulated heavy lines. The dashed line represents the difference between block (furnace or heater) and sample temperatures. Analogous curves can be derived for T_r and $\Delta T = T_r - T_s$. Small samples can be studied by TMDSC over at least one order of magnitude of change in time scale [8].

Experiments with modulation and an underlying linear heating rate as described by Eq. (4) have two time scales. One is due to the constant, underlying heating rate. The other is due to modulation with a temperature amplitude of $\pm A$. Fig. 1 is, again, a typical example. Each of the two time-dependent temperature changes can be used for the measurement of heat capacity. As long as the heat capacity can be treated as independent of time and temperature over one modulation cycle and amplitude, both evaluations give the same result. Outside of transitions or chemical reactions this is usually the case.

The determination of the heat capacity from modulation alone is carried out by a pseudo-isothermal analysis. The effect of modulation is separated for this analysis from the underlying change in temperature due to the heating rate $\langle q \rangle$ seen in Fig. 1. The instantaneous change in ΔT due to modulation, is given by $\Delta T(t) - \langle \Delta T \rangle$, where the average $\langle\ \rangle$ is, as before, carried always over $\pm 1/2\ p$, so that any sinusoidal effect averages to zero and the difference gives the required effect due to modulation alone. Evaluation of the calibration constant and the maximum amplitude of the temperature difference, A_Δ, which is proportional to the maximum heat flow amplitude A_{HF}, gives the heat capacity [6]:

$$mc_p = \frac{A_\Delta}{A}\sqrt{\left(\frac{K}{\omega}\right)^2 + C'2} = \frac{A_{HF}}{A} \times K' \qquad (5)$$

where A and ω are the modulation parameters set at the beginning of the experiment and described in Eq. (4), and C' is the heat capacity of the empty reference pan of identical mass to the empty sample pan. The calibration constant K is independent of modulation frequency and reference heat capacity. The commonly measured calibration constant K' changes for runs with different ω and C'. To account for the different frequencies (but not different C'), K' can be written as K''/ω. Eq. (5) represents the 'reversing' heat capacity. It can then be compared to the heat capacity measured from the underlying heating rate $\langle q \rangle$ alone, making use of the total heat flux $\langle HF \rangle$ or temperature difference $\langle \Delta T \rangle$, as calculated from Eq. (3) and seen in Fig. 1.

In case there is a difference between the result of Eqs. (3) and (5), this is called the 'nonreversing' heat capacity. Changes of the heat capacity with time can always be linked to irreversible effects, while temperature-dependent heat capacities are usually reversible. Both time and temperature changes of the heat capacity may contribute to the reversing and nonreversing parts.

A third experimental mode of measuring C_p by TMDSC is possible by keeping the average temperature, $\langle T \rangle$, constant, at T_0. This mode is called quasi-isothermal analysis [9]. To cover a range of temperature, separate experiments must be done at every T_0,

similar to the adiabatic analysis of Eq. (1). This analysis mode is more time consuming, but has the advantage that steady state can be awaited and many inaccuracies in separating the effects from the two time scales, avoided. The heat capacity is given in this case also by Eq. (5). Typically, runs of 20 min duration are made at each temperature and the last 10 min are used for data collection and analysis. Using one data point every 10 K, a range of 200 K can be covered in seven hours.

3. Experimental conditions of heat-capacity measurement

One of the basic conditions for any DSC measurement is a negligible temperature gradient within the sample [5]. If this were not so, the sample temperature would be uncertain and the measured ΔT would be influenced by the thermal conductivity of the sample. By reducing the temperature gradient within the sample to a negligible level, the heat flux into the sample calorimeter is governed only by the thermal conductivity and geometry of the surroundings [expressed by K of Eq. (3)] and the difference in temperature between heater and sample or reference as expressed by Newton's law: $dQ/dt = K(T_b - T_s)$. For TMDSC, one adds the condition that the maximum modulation amplitude A must be experienced by the entire sample calorimeter.

In standard DSC, a slightly larger temperature gradient within the sample will shift the measured (average) heat capacity to a lower temperature, but cause only a relatively small error since the heat capacity changes only slowly with temperature. In TMDSC, in contrast, one loses under conditions of incomplete modulation the volume which is not or only incompletely modulated, and thus experiences a more serious error. The conditions and calibration procedures, i.e. limits of p, A, and m were discussed earlier [9]. A reasonable initial set of parameters for present-day TMDSC is, perhaps, $p = 60$ s, $A = 1$ K, and $m = 10$ mg, to which an underlying heating rate $\langle q \rangle$ of up to 5K/min may be added. The limits should always be controlled by varying the sample mass to check for constant heat capacity. A standard DSC, in contrast, may measure up to 30 mg at a heating rate of up to 20 K/min for maximum precision.

The next condition for Eqs. (3) and (5) to hold, is the attainment of steady state. In Fig. 1 one can see that steady state is reached after ca. 200 s. More quantitatively, one may assume that a deviation of ±5% in sample temperature (and correspondingly less in ΔT) signals the attainment or loss of steady state. Mathematically, the deviation from steady state, Λ, can be expressed for the sample temperature and analogously for the reference temperature by [7]:

$$\Lambda = T_s(t) - T_0 - \langle q \rangle t + \langle q \rangle \frac{C_s}{K} - A[\sin(\omega t - \varepsilon)]$$
$$= \left[\langle q \rangle \frac{C_s}{K} + A\sin\varepsilon\right] e^{-Kt/C_s} \quad (6)$$

With the parameters of Fig. 1, $\Lambda \approx 3\exp(-t/50)$, and it takes ca. 200 s to reach the 5% value when starting the measurement from $T_b = T_s = T_r(t = 0)$. The approximate steady-state lag of the temperature due to the underlying heating rate is $\langle q \rangle C_s/K = 2.5$ K, i.e. it is the dominating effect under the given conditions. For large modulation amplitudes and small values of C_s/K and/or $\langle q \rangle$, the second term may well become more important.

Any subsequent, step-wise change in heat capacity causes a loss of steady state Λ that dies off with the exponential given by Eq. (6). If additional changes occur before steady state has been reached, simple additions show the overall effect because of the linearity of the heat-flux equations [7]. The occurrence of a glass transition over a limited temperature range may, for example, cause an increase in C_p of 10 J K^{-1} mol^{-1} at an overall heat capacity of the solid of ca. 20 J K^{-1} mol^{-1}. Assuming, furthermore, the glass transition occurs linearly over a temperature range of ca. 10 K (5% increase in heat capacity per degree Kelvin of temperature increase), Fig. 2 can be calculated by stepwise addition of the appropriate multiple terms derived from Eq. (6). The filled squares represent the increase in a lag-free experiment. The computed T_s shows the observed sample temperature, and the difference is the lag. The lag of 3 K in fixing a glass-transition temperature is, perhaps, still acceptable for common determinations of the glass transition. A deviation of the heat-capacity increase by more than 10% is, however, not acceptable. For the reporting of C_p for the ATHAS data bank [10], this error was in the past eliminated by extrapolation of the solid and liquid

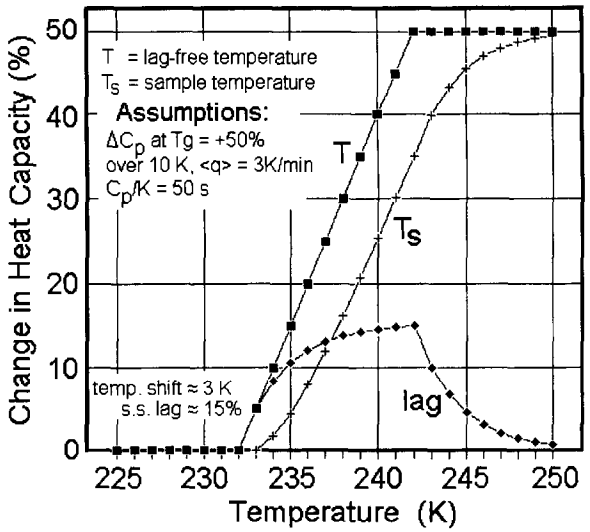

Fig. 2. Computation of lag on TMDSC in the glass-transition region. Actual measurements can be done with C_p/K as small as 1 s.

heat capacities to the glass-transition temperature, T_g. For integration of the heat capacities to enthalpy, it was assumed that a vertical increase of ΔC_p occurs at T_g. Applying the estimate of Fig. 2 to actual polymers like polystyrene or poly(ethylene terephthalate), two polymers that are often used as standards, one sees changes of heat capacity of 19 and 30% at the glass transition, i.e. their lags are closer to the 5% error in heat capacity. Similarly, a reduction of C_s can make heat-capacity measurements through the glass transition stay in steady state. For studies of the kinetics of the glass-transition values of C_s/K as small as 1 s have been used [11]. For highest precision of both, the kinetic data within the glass-transition region and the equilibrium heat capacity outside of the glass transition with ΔC_p at the glass transition, two sets of measurement are recommended. One with large C_s for the equilibrium solid and liquid heat capacities, and one with small C_s in the glass-transition region for the apparent, time-dependent heat capacities. Fig. 3(a) shows through the elliptical Lissajous figures that even in the glass-transition region practically lag-free measurements are possible. The Lissajous figures were taken for the second 10 min of four quasi-isothermal experiments and reveal sinusoidal modulation of the sample temperature and the heat flow [11]. A similar

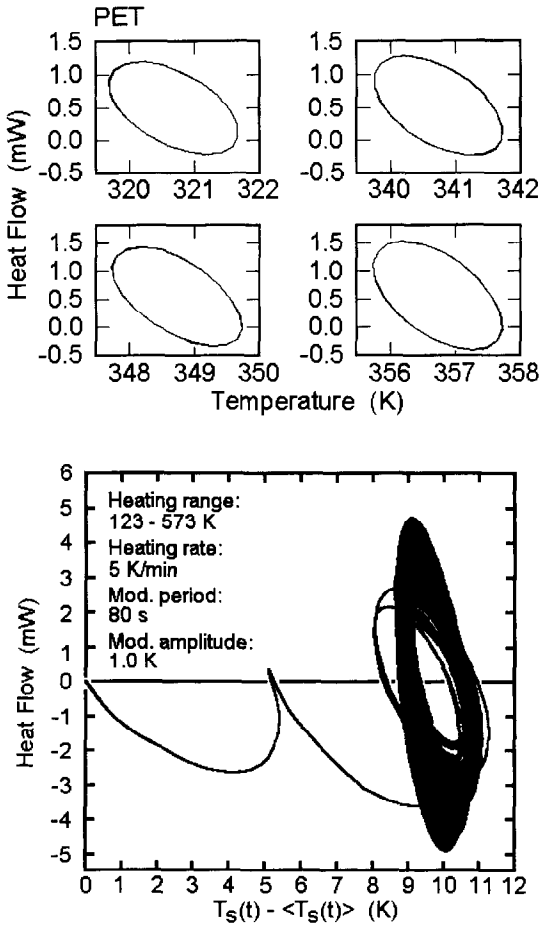

Fig. 3. Lissajous figures: (a) – recorded for four quasi-isothermal experiments in the glass-transition region of poly(ethylene terephthalate) [11]. Data for ten minutes after attainment of steady state; and (b) – data for a complete MDSC experiment with an Al_2O_3 sample using an underlying heating rate q [12].

test for a TMDSC experiment with an underlying heating rate $\langle q \rangle$ is reproduced in Fig. 3(b). In this case, the initial approach to steady state is clearly visible, and the change in steady-state condition due to the increase in heat capacity over the wide temperature range can be seen by the continued expansion of the steady-state ellipse. Details about the experimentation are in [12].

A linear increase in heat capacity causes a deviation from steady state and can be assessed by the integral of Eq. (6) from time zero to ∞ with the preexponential factor C_p (in % per K) $\times$ $\langle q \rangle$ (in K/s) (assuming small

modulation effects) [7]:

$$A = \langle q \rangle \left(\frac{dC_p}{dT}\right) \int_0^\infty e^{-Kt/C_s} dt' = \langle q \rangle \left(\frac{dC_p}{dT}\right) C_s/K \tag{7}$$

From this estimate, one can see that a change in heat capacity of less than 2%/K is within the chosen error limit of 5%. A typical increase of the heat capacity per kelvin in the solid state is, for example, 0.4% (polystyrene from (200–350 K), i.e. typical changes in heat capacity with temperature give negligible losses of steady state. By adjusting the sample mass, even steeper slopes of the apparent heat capacity as seen during premelting can be analyzed, and qualitative interpretation may be possible to levels as high as (25–50)% change in heat capacity per kelvin. Also, one must remember, that the heat of transition determined from the total heat flow is correct, even when steady state is lost while using the 'baseline method' [5,13].

A special problem in calibrating TMDSC is the correction for asymmetry, observed when running identical sample and reference calorimeters. Eq. (5) indicates that positive and negative deviation due to asymmetry would result in the same effect. A simple solution to this problem involves the introduction of a known asymmetry by using a somewhat heavier sample pan, so that the asymmetry remains positive over the whole temperature range of interest [14].

A final problem involves the question of temperature calibration. An attempt to calibrate with small amounts of indium revealed that calibration on heating and cooling cycles show only small differences for the onset of melting and crystallization at different positions of the modulation cycle [15]. It is of particular interest that, for small amplitudes of modulation, melting may be incomplete so that recrystallization shows no supercooling. It may thus not be necessary to switch to special calibrants of low supercooling.

The result of a measurement of heat capacity of poly(ethylene terephthalate), PET, including glass and melting transitions is shown in Fig. 4. Both, a standard DSC trace (line of intermediate thickness) and quasi-isothermal TMDSC in 2 K steps (thick line) is shown [16]. The heat capacity agrees well with the expected values from the data bank [10], based on adiabatic

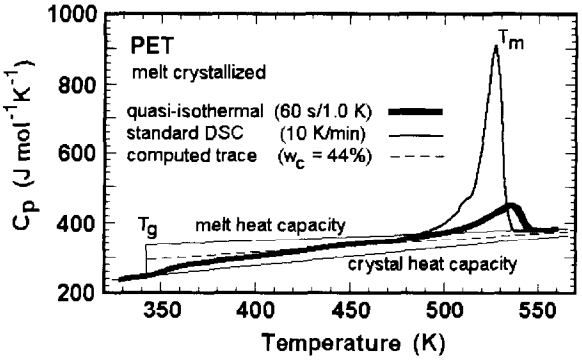

Fig. 4. Standard DSC and TMDSC curves of melt-crystallized PET. The DSC curve is of intermediate thickness, the TMDSC curve, heavy. The additional thin lines indicate data-bank information, the broken line represents the computed heat capacity for a sample of 44% crystalline PET.

calorimetry and standard DSC (thin lines). The glass transition has practically no hysteresis, as expected for semicrystalline PET [17]. A gradual loss of the rigid amorphous fraction seems to occur, as indicated by the eventual matching of calculated semicrystalline (dashed thin line) and measured heat capacities. The initial melting is almost fully irreversible. There is, however, a small reversible portion of the fusion. It changes with sample preparation and seems to indicate that, on a molecular level, melting of polymers is reversible. The extension of the quasi-isothermal melting/crystallization to higher temperatures than in the standard DSC experiment is caused by annealing, occurring during the sequences of 20 min measurements. Full details will be displayed in Ref. [16].

4. Apparent heat capacities within the glass transition

The apparent reversing heat capacity of amorphous polystyrene as a function of modulation frequency is shown in Fig. 5 [11]. The data were computed from kinetics parameters, obtained from quasi-isothermal measurements at different modulation amplitudes after extrapolation to $A = 0$. The apparent heat capacity calculated in this fashion represents the first harmonics of the Fourier analysis of the TMDSC heat flow signal. The higher harmonics are small and are neglected.

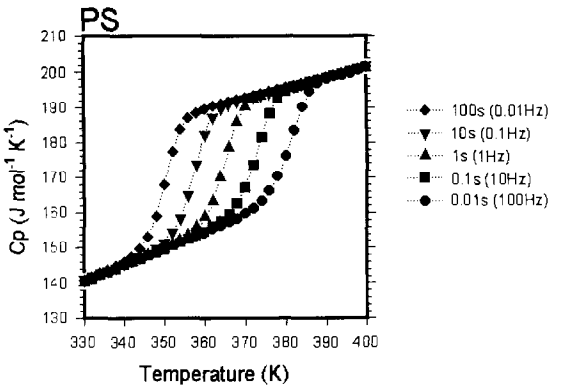

Fig. 5. Apparent heat capacity of polystyrene as a function of frequency (data extrapolated to zero modulation amplitude and extended beyond the frequency range of MDSC).

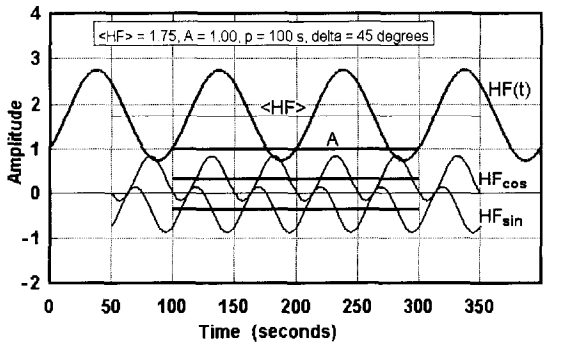

Fig. 6. Simulation of the MDSC software treatment of a sinusoidal heat flow, $HF(t)$, of amplitude $A = 1.00$ (arbitrary unit), superimposed on a constant heat flow $\langle HF \rangle$ of 1.75. The phase lag relative to the reference frequency is 45°. Shown also are the two Fourier components of the heat flow that are used to compute the amplitude: $A = 2[\langle HF_{cos} \rangle^2 + \langle HF_{sin} \rangle^2]^{1/2}$.

To better understand the kinetic effect of the glass transition as assessed by TMDSC with an underlying heating rate, i.e. involving two time scales, a two-step modeling routine was developed. First, the evaluation of the changing heat flow by the MDSC software was simulated on a Lotus 1-2-3™ spread sheet [18]. Fig. 6 shows the result of the addition of a constant heat flow of 1.75 units and a modulated heat flow of a maximum amplitude of 1.00 at a phase lag of 45° to the reference phase ωt. Feeding any heat flow into the modeling software will show the expected MDSC result in form of the first harmonic of the Fourier analysis of the instantaneous heat flow at time t, $HF(t)$. Next, the glass-transition kinetics was assumed to be of the first order, as can be derived from irreversible thermodynamics for any process close to equilibrium or from the hole theory [5]. The details of this simulation are given in [19] and are briefly discussed in the following.

The heat capacity is separated into the part arising from the vibrational contributions C_{po}, which are known from the heat capacity of the glass and crystal [10], and the part from the large-amplitude motion, simply called the hole contribution C_{ph} [20]. The number of holes is called N and is equated with the internal variable that changes during the glass transition. The equilibrium number of holes is N^*, and the heat of formation of one mole of holes is ε_h, a quantity available from the increase in heat capacity at the glass transition [20]. At equilibrium, the heat capacity is:

$$C_{p(liquid)} = C_{p_0} + \varepsilon_h \left(\frac{dN^*}{dT} \right) \tag{8}$$

Creation, motion, and destruction of holes are the slow, cooperative processes that account for the difference in heat capacity between liquid and solid. Deviations from Eq. (8) occur if the measurement is carried out faster than permitted by the kinetics of the changes in the number of holes. One writes then the first-order kinetics expression as [20]:

$$\left(\frac{dN}{dt} \right) = \frac{1}{\tau} (N^* - N) \tag{9}$$

with N representing the instantaneous number of holes and τ the relaxation time for the formation of holes. The mathematical solution of Eq. (9) is rather difficult since both, τ and N^* are temperature-, and thus time-dependent [21]. It is easier to solve Eq. (9) numerically since all activation parameters are available through quasi-isothermal experiments in the glass-transition region [11]. For the limited temperature range of the glass transition, one can assume that both N^* and τ have an Arrhenius-type temperature dependence. The glass-transition range is then divided into time intervals of one second, each with a constant N_i^* and an average value of the temperature-dependent relaxation time τ_i^* with i representing the running index of time. The value of N at the end of the one-second interval is given after integration over the small

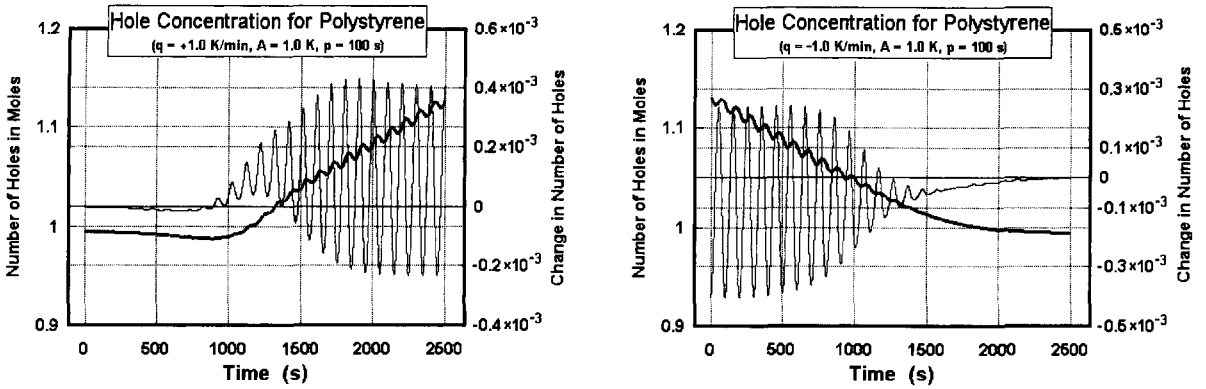

Fig. 7. Number of holes and their change on (a) – heating, and (b) – cooling in TMDSC, using data derived from quasi-isothermal analysis.

one-second intervals by:

$$N_i = N_i^* - (N_i^* - N_{i-1})\exp(-t/\sqrt{\tau_i \times \tau_{i-1}}) \tag{10}$$

Because of the one-second intervals, i is equal to t; N the time- and temperature-dependent number of holes, is obtained by adding the increments $N_i - N_{i-1}$ calculated from Eq. (10) from the beginning of the experiment to time i. On cooling from the equilibrium liquid, the value of N_o is set equal to N^*. On heating from the glassy state N_o is set equal to N^* at the fictive temperature. Fig. 7 shows a sample calculation of N, N^*, and ΔN on (a) heating and (b) cooling. For the chosen example, the ultimately frozen number of holes gives a value of N that corresponds to the equilibrium number of holes at 340.34 K, the fictive temperature. Subsequent heating of such glass shows a hysteresis behavior (Fig. 7(a), enthalpy relaxation) [5,20].

Using the heat flow $HF(t)$ that corresponds to ΔN of Fig. 7, one can calculate the various Fourier components using the simulation routine illustrated in Fig. 6. In Fig. 8 the results can be seen [19]. The heavy curves show the total heat capacity $C_{p(total)}$ computed from Eq. (3). The continuously decreasing curve with very little residual modulation is the reversing heat capacity computed using the pseudo-isothermal analysis (Eq. (5)). It is surprising that there is still some modulation evidence in the glass-transition region since Fig. 6 suggested that the MDSC software would remove it. A detailed analysis with larger modulation

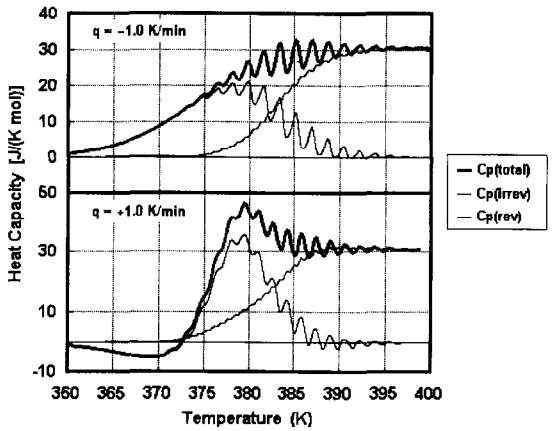

Fig. 8. Computed heat capacity on cooling (upper curves) and heating (lower curves). The curve C_p(irrev) is the difference between the total and the reversing heat capacity. Computed from quasi-isothermal activation parameters for a 1.0 K temperature modulation and a modulation period of 100 s.

amplitudes has shown that this remaining effect, which is largely lost by further smoothing, is due to a frequency shift of the modulation, resulting from the summation of the two time effects: the constant underlying cooling or heating rates and the modulation. This summation is similar to the Doppler effect on the sound frequency of a moving source [19]. More detailed analysis of the kinetic equation (Eq. (9)) reveals a certain second-harmonic contribution [19,21] that is excluded by the MDSC software from the reversing heat capacity and is, thus, added wrongly to the nonreversing C_p. It can, however, easily be

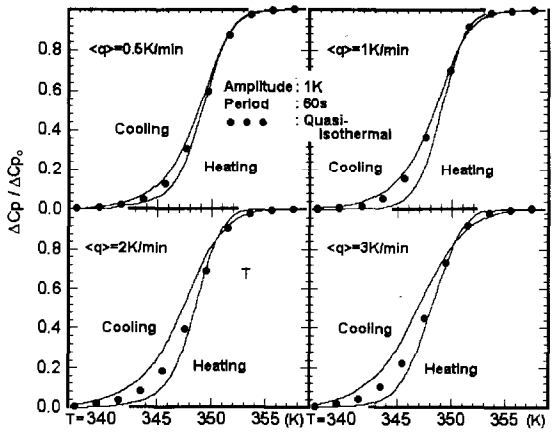

Fig. 9. Experimental data on TMDSC of amorphous poly(ethylene terephthalate) at the indicated run parameters. The central points are quasi-isothermally measured, the curves refer to TMDSC for different underlying heating and cooling rates $\langle q \rangle$.

calculated by a full Fourier analysis. The remaining oscillation in the total heat flow shown in Fig. 8 also produces nonzero higher harmonics [19]. Before a quantitative interpretation of reversing and nonreversing heat capacity is possible, it is thus necessary to analyze the process in more detail with data from quasi-isothermal analyses.

A comparison of the quasi-isothermal heat capacity with pseudo-isothermal analysis of the heat capacity from TMDSC runs was shown for polystyrene in [22] and is illustrated in Fig. 9 as a function of heating and cooling rates for amorphous poly(ethylene terephthalate)s [23]. It can be seen that, for low heating rates, the three measurements approach each other. For the first time it is, thus, possible to extract data for the apparent heat capacity in the glass-transition region on heating as well as on cooling runs. This avoids the otherwise tedious and not so precise extrapolation to the intersection of extrapolated liquid and glassy enthalpies [5].

At higher heating rates, small deviations occur. Close to the liquid state the simple kinetics, discussed here, describes the deviations quantitatively [22]. To agree with the experimental data of Fig. 9 at lower temperatures, there must be a slower, 'self-retarding' freezing on cooling, than calculated, and an 'autocatalytic' speed-up of the unfreezing on heating. Such effect is not contained in the glass-transition kinetics of Eq. (9), irrespective of the assumed temperature dependence of N^* and τ. As usual, for all irreversible processes close to equilibrium, the simple first-order expression holds; further from equilibrium, however, it begins to deviate if the kinetics is only approximate. The analysis of glasses of different stability (thermal history) under identical MDSC conditions have also shown that the reversing heat capacity curves become sharper with higher stability of the initial sample (lower fictive temperature) [8]. Mathematically, a self-retarding kinetics on approaching the final state by decreasing the number of holes and an autocatalytic kinetics on approaching the final state by increasing the number of holes is generally described by the Tool–Narayanaswamy–Moynihan equation [22]. It was also observed by cyclic dynamic differential thermal analysis (DDTA) [20] that the enthalpy relaxation occurs over a narrower temperature range than expected from an Arrhenius-type relaxation time τ. Such narrower, nonexponential relaxation excludes the introduction of a distribution of hole sizes to improve the fit between calculation and experiment, but suggests a cooperative process. To correct the analysis, the Arrhenius equation is usually replaced by the Kohlrausch–Williams–Watts stretched exponential [22]. Final fitting is then accomplished by introduction of a distribution of relaxation times. Even for only one relaxation time, such description needs three additional constants. Using assumed values, in a modeling approach similar to the one used in this research, Hutchinson could show that, indeed, the apparent heat capacities on heating and cooling cross, as shown in Fig. 9 [24]. Perhaps it is possible to extract the additional parameters from the frequency and heating rate dependence of the characteristic cross-over points in Fig. 9. All of these observations point to the necessity to develop a better, cooperative kinetics for the description of the glass transition.

5. Apparent heat capacity within melting/crystallization and chemical reactions

Melting and crystallization need or produce much larger heat flows than needed for changing the temperature. Polyethylene, for example, has a heat of fusion of 4.11 k J mol^{-1}, compared to a heat capacity of ca. 35 J K^{-1} mol^{-1} in the melting region [10]. If the heat of fusion needs to be absorbed over a

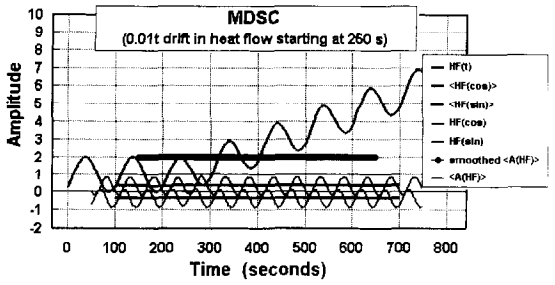

Fig. 10. Modeling of a linearly increasing heat flow similar to Fig. 6. The heat flow starts with a value of 1.0 (arbitrary unit) and increases after 250 s linearly. Modulation occurs with $A(HF)$ of 1.0 units. The averaged and smoothed maximum reversing heat-flow amplitudes are moved +1.0 unit on the ordinate for clarity.

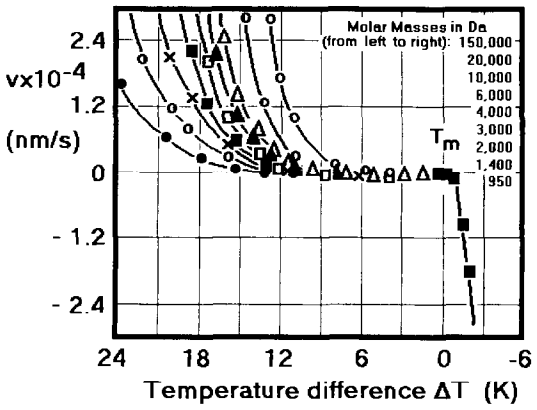

Fig. 11. Linear crystallization/melting rates of poly(oxyethylene) illustrating the expected irreversible polymer melting behavior [27].

temperature range of 1.0 K to stay in equilibrium, the heat flow would have to be more than 100 times larger than for a heat capacity measurement. For chemical reactions this discrepancy is even larger. The main problem for TMDSC is, thus, to stay in steady state, so that the derived equation for the heat capacity can also be used to assess the larger latent heat exchange. Again, the total heat flow can be integrated over a range of temperature where steady state was lost, and then calculated, using the baseline method [5]. To follow the melting and crystallization kinetically, small samples must be used, as outlined for the discussion of Eqs. (6) and (7).

The next problem is linked to the degree of reversibility of melting, crystallization or chemical reaction. As long as the latent heat is exchanged far from equilibrium, it will, once initiated, not follow the modulation, as is shown in the modeling of Fig. 10 [18]. In this case a linearly increasing heat flow is added to the modulation, as may be seen in a beginning oxidation or evaporation. The modulation shows that a complete separation is possible since the added change is not influencing the modulation. Heat capacity can in such cases be measured in the presence of large irreversible heat effects. This separation was discovered early [4] and is one of the major advantages of TMDSC: Effects that cannot be modulated are rejected from the reversing measurement as long as steady state and negligible temperature gradient within the sample are maintained. Examples of measurement of heat capacity in the presence of cold crystallization as in poly(ethylene terephthalate) have been shown in many laboratories [4,17]. Oxidation was illustrated to be separable from heat capacity measurements for one of the fullerenes [25] and for the study of decomposition of petroleum products [12], and a full analysis of heat capacity in the presence of curing of a thermoset was carried out [26], to name just three examples.

More complicated is the assessment if the latent-heat-producing process is fully or partially reversing. In this case, small sample masses must be used to maintain favorable measuring conditions. An exciting result is displayed in Fig. 4 for the melting of PET. It shows in its quasi-isothermal analysis that even for polymers a small amount of the melting is reversible. Comparing these data with a typical melting/crystallization study on poly(oxymethylene) in Fig. 11, one can see that there is a 6 K metastability gap between melting and crystallization, i.e. either process should be fully nonreversing as long as the modulation amplitude is less than ±3 K [27]. The metastability gap was ascribed to the lack of molecular nucleation in this temperature range [28]. Besides, from melting rate studies this molecular nucleation could be documented by rejection of fractions of macromolecule from growing crystals of larger molar mass below their melting temperature, which proved the existence of a reversible process at this lower than equilibrium melting/crystallization temperature. The process was called the 'molecular nucleation' [29,30]. This reversing process seems to be directly observable

in the quasi-isothermal experiment of Fig. 4. Tedious experiments with DSC and dissolution could already show that, for polyethylene, a small fraction of reversibly melting and crystallizing material could not be extracted from the sample, i.e. it was still attached to the crystals [31,32]. It seems that TMDSC may permit a quantitative analysis of this reversible melting fraction. We speculate that partially melted segments (in steady state) can – by minor reversal in temperature – recrystallize [16]. This fraction of the polymer participating in the reversing melting is strongly morphology- and processing-dependent, and may become a valuable characterization tool for the polymer structure.

An even more difficult topic involves the separation of simultaneously occurring exothermic and endothermic processes. The qualitative observation involves variation of the modulation scheme from heating and cooling to heating-only or cooling-only. Much still remains to be done for this important topic to become quantitative. It is hoped that the Fifth Lähnwitz Seminar will shed light on this and other TMDSC topics which are on the verge of becoming valuable new tools for materials characterization.

6. Conclusion

Temperature-modulated DSC allows two methods for measurement of heat capacity. The quasi-isothermal method without an underlying heating rate allows the evaluation of the reversing component, the pseudo-isothermal analysis method permits a simultaneous evaluation of reversing and nonreversing parts of the heat capacity. For heat capacities that change substantially during the time and temperature range of a modulation cycle, reversing and nonreversing heat capacities are not fully equivalent to reversible and irreversible heat capacities. The reversible and irreversible heat capacities may, however, be computed from the TMDSC data under proper experimental conditions and with knowledge of the proper kinetics, as was shown for the analysis of the glass transition. In many cases, the separation of heat capacity from transition effects can be accomplished. Even transitions with larger latent heats can be separated from the heat-capacity measurement and analyzed to give detailed insight into the molecular processes, establish kinetic parameters, and may also permit the separation of overlapping exothermic and endothermic processes.

Acknowledgements

This work was supported by the Division of Materials Research, National Science Foundation, Polymers Program, Grant # DMR 90-00520 and Oak Ridge National Laboratory, managed by Lockheed Martin Energy Research Corp. for the U.S. Department of Energy, under contract number DE-AC05-96OR22464. Some support came also from TA Instruments Inc. and ICI Paints.

References

[1] W. Nernst, Ann. Physik, 36 (1911) 395.
[2] E.S. Watson, M.J. O'Neill, J. Justin and N. Brenner, Anal. Chem., 36 (1964) 1233.
[3] E. Gmelin, Thermochim. Acta, 1997, this issue.
[4] M. Reading, D. Elliot, V.L. Hill, Thermal Anal J., 40 (1993) 949; P.S. Gill, S.R. Sauerbrunn and M. Reading, J. Thermal Anal., 40 (1993) 931; M. Reading, Trends in Polymer Sci., 8 (1993) 248.
[5] B. Wunderlich, Thermal Analysis, Academic Press, Boston, MA, 1990.
[6] B. Wunderlich, Y. Jin and A. Boller, Thermochim. Acta, 238 (1994) 277.
[7] B. Wunderlich, A. Boller, I. Okazaki and S. Kreitmeier, Thermochim. Acta, 282/283 (1996) 143.
[8] A. Boller, C. Schick and B. Wunderlich, Thermochim. Acta, 266 (1995) 97.
[9] A. Boller, Y. Jin and B. Wunderlich, J. Thermal Analysis, 42 (1994) 307.
[10] B. Wunderlich, Pure and Applied Chem., 67 (1995) 1919; U.Gaur, S-f. Lau, H-C. Shu, B.B. Wunderlich, M. Varma-Nair, and B. Wunderlich, J. Phys. Chem. Ref. Data, 10 (1981) 89, 119, 1001, 1051; 11 (1982) 313, 1065; 12 (1983) 29, 65, 91; 20 (1991) 349. See also our WWW site (http://funnelweb.utcc.utk./~athas).
[11] B. Wunderlich, Pure and A. Boller, Shaheer A. Mikhail (Ed.), Proc. 24th NATAS Conf, San Francisco, CA, Sept. 10–13, 1995, pp. 136–141. Full version by A. Boller, I. Okazaki and B. Wunderlich, Thermochim. Acta, 284 (1996) 1.
[12] M. Varma-Nair, H.S. Aldrich and B. Wunderlich, J. Thermal Analysis, 46 (1996) 879.
[13] T. Ozawa and K. Kanari, Thermochim. Acta, 253 (1995) 183.
[14] A. Boller, I. Okazaki, K. Ishikiriyama, G. Zhang and B. Wunderlich, J. Thermal Analysis, 1997, to be published ; see also K. Ishikiriyama and B. Wunderlich, J. Thermal Analysis, 1997, to be published.

[15] K. Ishikiriyama, A. Boller and B. Wunderlich, J. Thermal Analysis, 1997, to be published.
[16] I. Okazaki and B. Wunderlich, Macromolecules, 30 (1997) 1758.
[17] I. Okazaki and B. Wunderlich, J. Polymer Sci., Part B: Polymer Phys., 34 (1996) 2941.
[18] B. Wunderlich, J. Thermal Analysis, 48 (1997) 207.
[19] B. Wunderlich and I. Okazaki, J. Thermal Analysis, 49 (1997) 57.
[20] B. Wunderlich, D.M. Bodily and M.H. Kaplan, J. Appl. Phys., 35 (1964) 95.
[21] B. Wunderlich, A. Boller, I. Okazaki and S. Kreitmeier, J. Thermal Analysis, 47 (1996) 1013.
[22] L.C. Thomas, A. Boller, I. Okazaki, and B. Wunderlich, Thermochim. Acta, 1997, in print.
[23] I. Okazaki, unpublished, experimental details as given in [17].
[24] Qualitative simulation, using the model described by Hutchinson, in this issue.
[25] Y. Jin, A. Xenopoulos, J. Cheng, W. Chen, B. Wunderlich, M. Diack, C. Jin, R.L. Hettich, R.N. Compton and G. Guiochon, Mol. Cryst. Liq. Cryst., 257 (1994) 235.
[26] G. Van Assche, A. Van Hemelrijck, H. Rahier and B. Van Mele, Thermochim. Acta, 268 (1995) 121.
[27] S.Z.D. Cheng and B. Wunderlich, J. Polymer Sci., Part BPolymer Phys., 24 (1986) 595.
[28] B. Wunderlich, Disc. Farad. Soc., 68 (1979) 239.
[29] B. Wunderlich and A. Mehta, J. Polymer Sci., Polymer Phys. Ed., 12 (1974) 255.
[30] A. Mehta and B. Wunderlich, Colloid and Polymer Sci., 253 (1975) 193.
[31] A. Mehta and B. Wunderlich, Makromolekulare Chemie, 175 (1974) 977.
[32] B. Wunderlich, Macromolecular Physics, Vol. 3, Crystal Melting, Academic Press, New York, 1980.